Article

Two-pion Bose-Einstein correlations in Au+Au collisions at $\sqrt{s_{NN}} = 3$ GeV in the STAR experiment

Anna Kraeva (for the STAR Collaboration) [1,2]

[1] National Research Nuclear University MEPhI (Moscow Engineering Physics Institute); annakraeva555@gmail.com
[2] Joint Institute for Nuclear Research

Abstract: The correlation femtoscopy technique makes it possible to estimate the geometric dimensions and lifetime of the particle emission region after the collision of ions. Measurements of the emission region characteristics not only at midrapidity, but also at the backward (forward) rapidity can provide new information about the source and make it possible to impose constraints on the heavy-ion collision models. This work is devoted to revealing the dependence of the spatial and temporal parameters of the emission region of identical pions in Au+Au collisions at $\sqrt{s_{NN}} = 3$ GeV from the fixed-target program of the STAR experiment. The extracted femtoscopic radii, R_{out}, R_{side}, R_{long}, $R^2_{out-long}$, and the correlation strength, λ, are presented as a function of collision centrality, pair rapidity and transverse momentum. Physics implications will be discussed.

Keywords: Correlation femtoscopy, quark-gluon plasma, boost-invariance

1. Introduction

The important goal of the high-energy heavy-ion collision experiments is to study the properties of quark-gluon matter and its description from the first principles of the fundamental theory of strong interactions - quantum chromodynamics (QCD) [1–4]. Collisions of heavy ions generate matter with different temperatures, T, and baryon chemical potential, μ_B, which allows to probe different regions of the QCD phase diagram [5–7]. The phase diagram contains regions where partonic degrees of freedom dominate — quark-gluon plasma (QGP), hadronic degrees of freedom dominate — hadronic gas, and a mixed phase. According to theoretical predictions [8–10], there is a first-order phase transition between the QGP and the hadronic phase at finite μ_B, as opposed to the crossover transition at μ_B close to zero. The point where the first-order phase transition ends is called the QCD critical point. Finding the critical point and phase transition in the QCD phase diagram is the main focus in beam energy scan programs. The beam energy scan (BES) programs at the Relativistic Heavy Ion Collider (RHIC, USA) provides opportunity to explore different regions of the QCD phase diagram from low μ_B and high T to high μ_B and low T. This allows us to study the properties of nuclear matter and find possible phase transition and critical point signals. BES-I finished collecting data in 2011 and now BES-II and FXT have completed high-statistics data-taking at high-μ_B. The BES-II program covers collision energies at $\sqrt{s_{NN}} = 7.7 - 27$ GeV in the collider mode [11] that corresponds to μ_B from 420 to 150 MeV. The Fixed-target (FXT) program of BES-II provides an access to Au+Au collisions at $\sqrt{s_{NN}} = 3 - 7.7$ GeV [12], which corresponds to μ_B from 720 to 420 MeV. The data collected during the BES-II include upgrade of inner time projection chamber iTPC and installation of new detectors such as eTOF and EPD. The upgrades improve the acceptance of the particle detection and identification as well as event plane resolution.

Measurements of the spatial and temporal structure of particle emission region play one of the key roles in understanding of the quark-gluon matter evolution. The short lifetime of the system makes it impossible to directly measure position and time of particle

Citation: Kraeva, A. Title. *Journal Not Specified* **2023**, *1*, 0. https://doi.org/

Received:
Revised:
Accepted:
Published:

emission. Using momentum correlations of particles provides opportunity to extract the information about the source shape and lifetime [13–18].

Pion correlations were observed in experiments studying proton-antiproton annihilations by G. Goldhaber, S. Goldhaber, W. Li and A. Pais in 1960s. They proposed to take into account Bose-Einstein statistics to describe the production of identical and non-identical pion pairs with small opening angles [21]. In 1970s, G. Kopylov and M. Podgoretsky [22–25] proposed to use the correlation function to study the space-time structure of the particle-emitting region and settled the basics for future femtoscopy technique. The momentum correlations are also influenced by the final state interactions (FSI) – Coulomb and strong [27–30]. The Coulomb interaction affects correlation function at very small relative momenta (on the order of two-particle system inverse Bohr radius) [31,32]. Momentum correlations also allows one to study the properties of strong interaction between particles (recent experimental results and review can be found in Refs. [33,34]. Using unlike-sign pair correlations it is possible to study the relative space–time asymmetries in particle emission or the final-state interaction parameters [35–37].

In heavy ion collisions, the produced particles are assumed to be approximately boost-invariant with respect to the beam direction (longitudinal) that provides model for an expanding system [38]. Boost-invariance means that the particle density does not depend on the rapidity and the correlations between particles in the final state was the same in any coordinate system transformed longitudinally by Lorentz transformations. Experiments show that a flat rapidity plateau was observed at high energies at midrapidity [39]. At lower collision energies the rapidity distribution of single particle has a Gaussian shape and the flat plateau disappears at midrapidity, while the distribution for particle pairs has not been studied at high statistics.

This work is devoted to the study of femtoscopic correlations of identical pion pairs in Au+Au collisions at $\sqrt{s_{NN}} = 3$ GeV in the Fixed-target program in the STAR experiment. The resulting femtoscopic parameters of the system are measured as a function of collision centrality, pair rapidity (y_{pair}) and transverse momentum (k_T).

2. Materials and Methods

2.1. The correlation femtoscopy

Correlations of two particles with small relative momentum make it possible to extract information about the emission source. The size of the emission region is estimated by constructing a three-dimensional correlation function, $C(\mathbf{q})$, which is formed by the ratio of the distributions of the relative momenta of the particles. The numerator, $A(\mathbf{q})$, is formed using pairs where both tracks come from the same event, and the denominator, $B(\mathbf{q})$, is formed using the event mixing method [15,22] such that the two tracks come from separate events. It is constructed as:

$$C(\mathbf{q}) = \frac{A(\mathbf{q})}{B(\mathbf{q})} , \tag{1}$$

where $\mathbf{q} = \mathbf{p_1} - \mathbf{p_2}$ is the relative momentum of the first and second particle from a pair, respectively. The numerator contains correlations due to quantum statistics (QS) and final state interactions (Coulomb and strong). Meanwhile, the denominator does not contain femtoscopic correlations.

The correlation function is sensitive to the spatiotemporal structure of the pion radiation source at kinetic freeze-out (the last stage of the collision evolution, when particles finish scattering on each other) and shows the size of the “homogeneity" region [40] from which particles fly out with the similar magnitude of velocities and direction. In this analysis, pairs of particles correspond to identical pions.

In the Bertsch-Pratt system [41,42], the relative momentum of a pair of particles is projected as follows into three directions *out*, *side* and *long*: q_{out} is pointing along the average transverse momentum of the particle pair $k_T = |(\mathbf{p_{T,1}} + \mathbf{p_{T,2}})|/2$, q_{long} is pointing along the beam axis, and q_{side} is perpendicular to the previous two. Analysis is performed in the longitudinal co-moving system (LCMS), where $p_{1,z} + p_{2,z} = 0$. The $p_{1,z}$ and $p_{2,z}$ are the projections of the momenta of the first and second particle onto the beam axis.

The Bowler-Sinyukov procedure [43–45] is used to fit the correlation function and extract the femtoscopic parameters:

$$C(\mathbf{q}) = N[(1-\lambda) + \lambda K(\mathbf{q})(1 + G(\mathbf{q}))], \tag{2}$$

where N is a normalization factor, λ is a coefficient that characterizes the strength of femtoscopic correlations, $K(\mathbf{q})$ is the Coulomb factor describing the Coulomb repulsion in the case of identical particles. The λ can be influenced by secondary particles born from resonance decays, which can be mistakenly identified as primary pions. The quantity $K(\mathbf{q})$ is the square of the Coulomb wave function integrated over the spherical Gaussian source. In this analysis, the Coulomb radius of 5 fm was used to calculate $K(\mathbf{q})$.

The term $G(\mathbf{q})$ represents the Gaussian source function and can be described by the following equation:

$$G(\mathbf{q}) = \exp(-q_o^2 R_o^2 - q_s^2 R_s^2 - q_l^2 R_l^2 - 2q_o q_s R_{os}^2 - 2q_s q_l R_{sl}^2 - 2q_o q_l R_{ol}^2), \tag{3}$$

where R_{out}, R_{side}, R_{long}, R_{ol}^2, R_{os}^2 and R_{sl}^2 are components of femtoscopic radii. In this analysis, R_{ol}^2 has a non-zero value and corresponds to the tilt of the correlation function in the $q_{out} - q_{long}$ plane. The R_{ol}^2 is expected to be positive for positive rapidities, cross zero at midrapidity, and become negative for negative pair rapidities. The other components R_{os}^2 and R_{sl}^2 are zeroed due to the symmetry.

2.2. *Experimental setup and analysis details*

Data from Au+Au collisions at $\sqrt{s_{NN}} = 3$ GeV from the FXT program of the STAR experiment at RHIC were analysed. The interaction probability between the beam and the target is 1 % (determined using the inelastic Au+Au cross section). The gold beam collided with a gold target 0.25 mm thick (density 1.93 g/cm^2) with a incident beam momentum of 3.85 GeV per nucleon in the laboratory frame. The target was installed inside the vacuum tube, 2 cm below its center, at a distance of 200.7 cm to the west of the center of the STAR detector.

In this analysis, events with reconstructed primary vertex were selected using the following selection criteria: $198 < V_Z < 202$ cm and $V_R = \sqrt{V_X^2 + V_Y^2} < 2$ cm, where V_z is the vertex position along the beam direction and V_R is the radial vertex position. Left panel in Fig. 1 shows the distribution of reconstructed position of collision vertex in the XY plane.

Collision centrality can be determined using the multiplicity of charged particles. To estimate centrality, primary tracks (tracks fitted to the reconstructed collision vertex) were used to determine multiplicity of charged tracks ($fxtMult$) in the FXT program. Right panel of Fig. 1 shows the $fxtMult$ distribution. The shaded areas show the ranges for $0-10$ %, $10-30$ %, $30-50$ % and $50-80$ % central collisions.

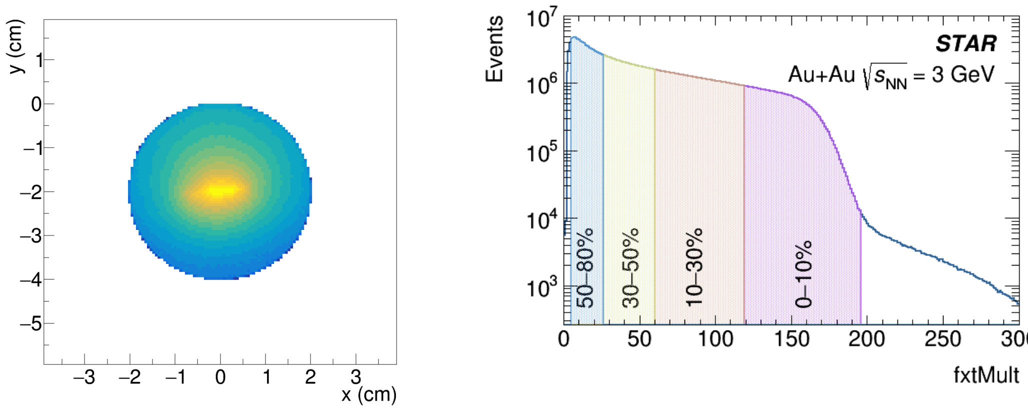

Figure 1. (left panel) Collision vertex in the XY plane. (right panel) The $fxtMult$ distribution.

The following cuts were used for track selection: pseudorapidity $-2 < \eta < 0$, more than 15 ionization points inside the Time Projection Chamber (TPC) and the distance of closest approach (DCA) to the primary vertex is less than 3 cm. The latter was introduced to reduce the contribution of non-primary pions.

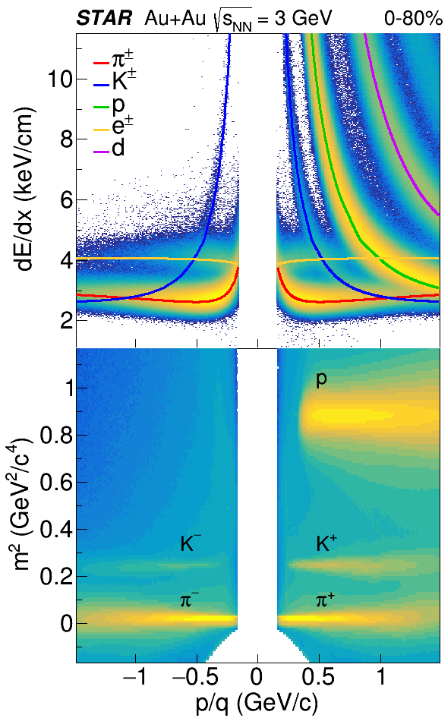

Figure 2. (top panel) The particle identification using dE/dx in the TPC. (bottom panel) The particle identification using m^2 from TOF.

Particle identification was performed utilizing ionization losses in TPC and time of flight in TOF. Figure 2 shows the distribution of ionization losses, dE/dx, in TPC (top panel) and the distribution of particle mass squared estimated via time of flight (bottom panel). The lines indicate theoretical calculations of particle ionization losses. The red, blue, green, yellow and violet color lines correspond to $\pi^{\pm}$, $K^{\pm}$, p, $e^{\pm}$ and d, respectively.

A combination of TPC and TOF was used in this analysis. In the region of low momentum ($0.15 < p < 0.55$ GeV$/c$) particle identification was performed by measuring dE/dx in the TPC for each track and comparing it with the expected value for each particle type i using the equation:

$$n\sigma_i = \frac{1}{\sigma_i}\log\left(\frac{dE/dx_{\text{measured}}}{dE/dx_{\text{expected},i}}\right), \tag{4}$$

where σ_i is the dE/dx resolution of the TPC.

The following selection criteria were used to identify pions: $|n\sigma(\pi)| < 2$, $|n\sigma(e, K, p)| > 2$, which suppresses contamination to pions from other particles.

At higher particle momentum ($0.55 < p < 1.5$ GeV$/c$) pions were selected using a combination of TPC and TOF. The particle tracks with $|n\sigma(\pi)| < 3$ and $-0.05 < m^2 < 0.08$ GeV$^2/c^4$, $|1/\beta - 1/\beta(\pi)| < 0.015$ estimated via TOF (β is the particle velocity) were assumed to be pions. The single-pion purity was estimated to be not lower than 98 %.

The correlation function is sensitive to detector effects such as track merging and splitting. These effects originate from the process of track reconstruction: one track can be reconstructed as two (track splitting), and two tracks are reconstructed as one (track merging). In the case of track splitting, the so-called false tracks affect the correlation function in the region of low relative momentum. To assess how track splitting affects correlation functions, the concept of Splitting Level (SL) is introduced:

$$SL = \frac{\sum\limits_{i=1} S_i}{Nhits_1 + Nhits_2}, \tag{5}$$

where $S_i = +1$ if only one track of a pair has a hit, $S_i = -1$ if both tracks of a pair have hits, $S_i = 0$ if no track has a hit in the detector plane. $Nhits_1 + Nhits_2$ represent the sum of the hits of the two tracks. For this analysis, a constraint of $-0.5 < SL < 0.6$ was applied, which suppresses the effect of track splitting on the correlation function.

On the other hand, the track-merging effect also affects the correlation function of identical pions. The fraction of merged hits (FMH) between two tracks was used to estimate the effect of track merging. The particle pairs with $FMH < 10$ % (that mostly eliminates the effect) were analysed.

The current analysis was split into two parts. First, we performed the rapidity-integrated analysis for pair transverse momentum ranges [0.15, 0.25], [0.25, 0.35], [0.35, 0.45], [0.45, 0.55], [0.55, 0.65] GeV$/c$. In the second part, the femtoscopic correlations were studied for the single k_T range of [0.15, 0.6] GeV$/c$ and for multiple rapidity ($y_{cm} - y_{pair}$) intervals: [0, 0.2], [-0.2, 0], [-0.4, -0.2], [-0.6, -0.4], [-0.8, -0.6]. Positively and negatively charged pion pairs are analysed separately. Figure 3 shows the two-pion acceptance, where the dashed lines correspond to the pair rapidity and transverse momentum intervals used in the study. A shift of pair rapidity by y_{cm} ($y_{cm} = 1.05$ for $\sqrt{s_{NN}} = 3$ GeV) allows to boost the kinematics from laboratory to the center of mass frame.

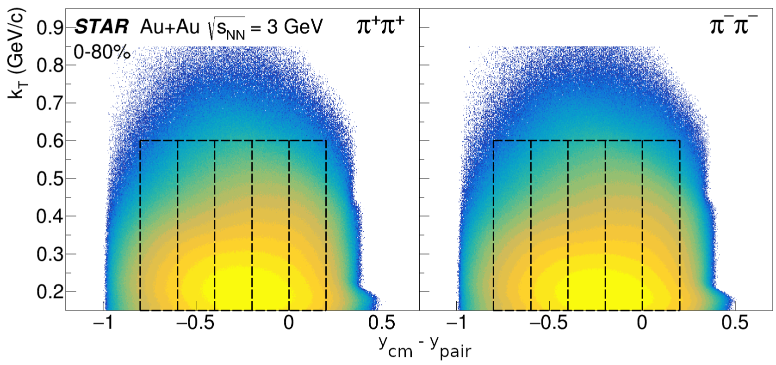

Figure 3. Acceptance of positively (left panel) and negatively (right panel) charged pion pairs for Au+Au collisions at $\sqrt{s_{NN}} = 3$ GeV. Dashed lines denote the selected rapidity windows for the rapidity-differential analysis.

To extract the femtoscopic parameters (R_{out}, R_{side}, R_{long}, λ, $R^2_{out-long}$), the equation 2 was used to fit the correlation functions.

2.3. Systematic uncertainties

The next sources of systematic uncertainties are considered in this work: radius variation of Coulomb interaction between particles, correlation function fit range, fraction of merged tracks (FMH), and the splitting level (SL). Table 1 shows default parameters and their variations.

Table 1. Systematic sources and their variations

Systematic source	Default	Variations
Splitting Level (SL)	$-0.5 \leqslant SL \leqslant 0.6$	$-0.5 \leqslant SL \leqslant 0.4$; $-0.5 \leqslant SL \leqslant 0.8$
Fraction of merged tracks (FMH)	$FMH \leqslant 0.1$	$FMH \leqslant 0$; $FMH \leqslant 0.2$
Fitting range	$[-0.25, 0.25]$	$[-0.2, 0.2]$; $[-0.3, 0.3]$
Coulomb radius	5 fm	3 fm; 7 fm

The Barlow test was used to calculate total systematic uncertainty. A variation of a parameter, giving a value R^{var}, where the value with the default choice for the parameter is R^{def}, introduces a systematical uncertainty if the difference between the default value and the variation is larger than their statistical error difference:

$$|R^{def} - R^{var}| > \sqrt{|\sigma^2[R^{def}] - \sigma^2[R^{var}]|} \tag{6}$$

Systematic uncertainty from i-th source (for example, SL) for j-th variation passing Barlow test [46] is:

$$\sigma^j_{sys,i}[R] = \sqrt{|R^{def} - R^{var}|^2 - |\sigma^2[R^{def}] - \sigma^2[R^{var}]|} \tag{7}$$

Systematic uncertainty from i-th source (for example, SL) with m cut variations (for example, $-0.5 \leqslant SL \leqslant 0.4$; $-0.5 \leqslant SL \leqslant 0.8$) is:

$$\sigma_{sys,i}[R] = \sqrt{\left[\sum_{i=1}^{m} (\sigma^j_{sys,i}[R])^2\right] / m} \tag{8}$$

The total systematical uncertainty from n systematic sources calculated as:

$$\sigma^{tot}_{sys}[R] = \sqrt{\sum_{i=1}^{n} \sigma^2_{sys,i}[R]} \tag{9}$$

Systematic errors of femtoscopic parameters were calculated for each bin of centrality, k_T, and pair rapidity. Table 2 shows sources of systematic uncertainty and its typical values.

Table 2. Sources of systematic uncertainty and its typical values

Systematic source	R_{out}	R_{side}	R_{long}
Splitting Level (SL)	0.1%	0.1%	0.2%
Fraction of merged tracks (FMH)	0.3%	0.2%	0.2%
Fitting range	0.2%	0.2%	0.3%
Coulomb radius	2.6%	1.2%	0.7%
Total	2.6%	1.2%	0.8%

3. Results

In the rapidity-integrated analysis, correlation functions were studied for several k_T ranges ([0.15, 0.25], [0.25, 0.35], [0.35, 0.45], [0.45, 0.55], [0.55, 0.65] GeV$/c$) and 3 centrality classes ($0-10\%$, $10-30\%$, $30-50\%$ central Au+Au collisions). Correlation functions were constructed and fitted by Eq. 2 separately for positive and negative pion pairs. Figure 4 shows an example of correlation function and fit projections for pion pairs with $0.15 < k_T < 0.25$ GeV$/c$ measured for $0-10\%$ central collisions. Red and blue circles show projections of the three-dimensional correlation function onto the *out*, *side* and *long* axes for $\pi^+\pi^+$ and $\pi^-\pi^-$, respectively. The red and blue lines show the fit projections of Eq. 2 to the correlation functions of $\pi^+\pi^+$ and $\pi^-\pi^-$, respectively. For each projection (q_{out}, q_{side}, q_{long}) shown, the other components of relative momentum are integrated over the range ± 0.05 GeV$/c$.

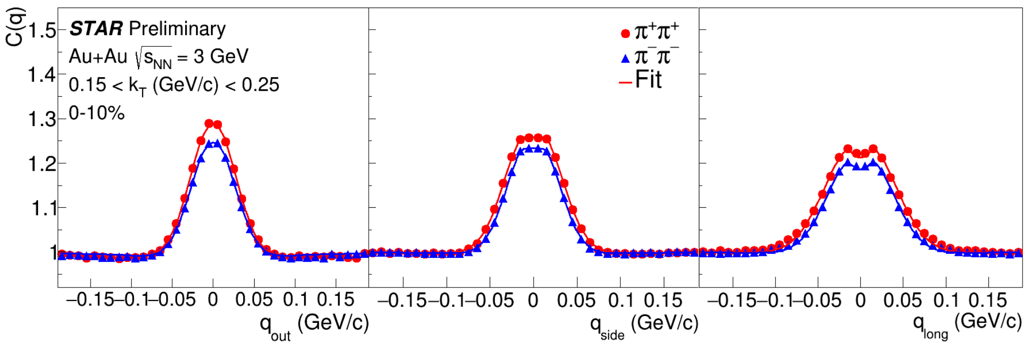

Figure 4. Correlation functions of positive (red markers) and negative (blue markers) pions with a centrality of 0–10% in the range $0.15 < k_T < 0.25$ GeV$/c$ at $\sqrt{s_{NN}} = 3$ GeV in Au+Au collisions. In each case the other components are projected over ± 0.05 GeV$/c$.

Figure 5 shows the R_{out}, R_{side} and R_{long} as a function of k_T for the 0–10% central collisions. R_{out}, R_{side} and R_{long} are shown as red, blue and black markers, respectively. Filled and empty markers correspond to the negative and positive pion pairs, respectively. The shaded area represents systematic uncertainty estimated for each data point.

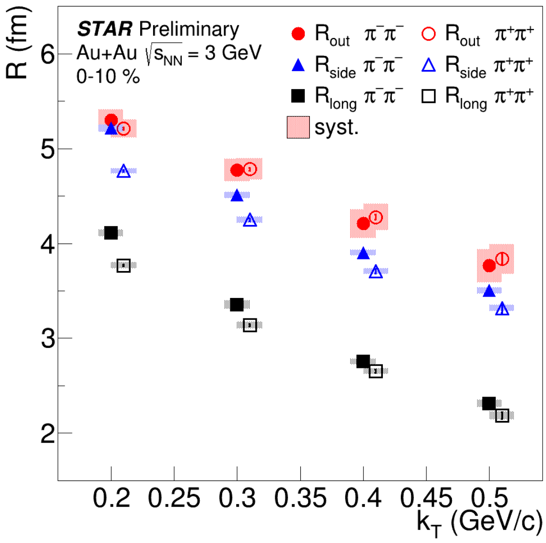

Figure 5. Extracted pion source radii (R_{out}, R_{side}, R_{long}) as a function of the k_T for the 0–10% central Au+Au collisions at $\sqrt{s_{NN}} = 3$ GeV.

In the differential analysis, correlation functions were constructed in different rapidity ($y_{cm} - y_{pair}$) intervals: [0, 0.2], [-0.2, 0], [-0.4, -0.2], [-0.6, -0.4], [-0.8, -0.6] (see Fig. 3) for $0.15 < k_T < 0.6$ GeV$/c$ and 0–10 %, 10–30 %, 30–50 % centrality classes. The femtoscopic parameters are extracted from fitting Eq. 2 to the correlation functions. Figure 6 shows the R_{out}, R_{side}, R_{long}, λ, $R^2_{out-long}$ dependence on $y_{cm} - y_{pair}$. Filled markers refer to negative pion pairs, empty ones - to positive ones. Black, red and blue markers represent 0-10 %, 10-30 % and 30-50 % central collisions, respectively. Gray markers are the measured results mirrored with respect to midrapidity ($y_{cm} - y_{pair} = 0$). Rectangular empty areas represent systematic uncertainties.

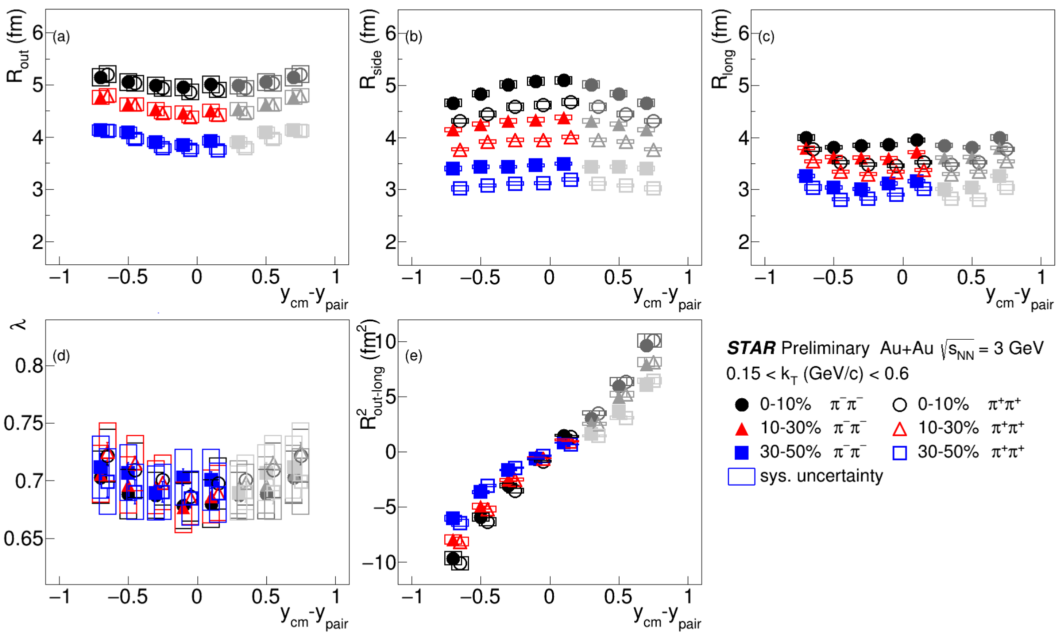

Figure 6. The R_{out} (a), R_{side} (b), R_{long} (c), λ (d), $R^2_{out-long}$ (e) as a function of pair rapidity ($y_{cm} - y_{pair}$). The values for 0–10%, 10–30%, 30–50% centrality classes of Au+Au collisions at $\sqrt{s_{NN}} = 3$ GeV are depicted as black circles, red triangles and blue squares, respectively. Filled markers represent the data for $\pi^-\pi^-$ and empty markers correspond to $\pi^+\pi^+$.

4. Discussion

In rapidity-integrated analysis an example of the constructed correlation functions for $\pi^+\pi^+$ and $\pi^-\pi^-$ for the most central collisions is shown in Fig. 4. The peak of correlation functions for $\pi^+\pi^+$ is larger than that for $\pi^-\pi^-$ at $0.15 < k_T < 0.25$ GeV/c and for 0-10 % central collisions. The difference between the extracted femtoscopic parameters for positive and negative pion pairs is most visible for R_{side} and R_{long} that may be due to the influence of residual electric charge and different resonance decay contributions.

The extracted femtoscopic parameters (R_{out}, R_{side} and R_{long}) are studied as a functions of pair transverse momentum and shown in Fig. 5. The femtoscopic radii for both positive and negative pion pairs decrease with increasing k_T. This can be explained as a decrease of the particle emission region due to the transverse flow. A difference of the femtoscopic radii of positive and negative pions, extracted in the side and long projections, is observed.

Figure 6 shows rapidity dependence of femtoscopic parameters (R_{out}, R_{side}, R_{long}, λ, $R^2_{out-long}$) for $0-10\%$, $10-30\%$ and $30-50\%$ central collisions. The R_{out}, λ and R_{long} increase with moving away from the midrapidity, while R_{side} follows the opposite trend. The values of R_{out}, λ and $R^2_{out-long}$ are similar for $\pi^+\pi^+$ and $\pi^-\pi^-$. The values of R_{side} for $\pi^-\pi^-$ are systematically larger than that for $\pi^+\pi^+$ for all centrality classes and pair rapidity intervals studied. The R_{side} represents the geometrical size of the particle emission source. Hence, negative pions are emitted from homogeneity regions with larger sizes than those of positive pions. The R_{out} reflects the geometrical size and is sensitive to the particle emission duration. Different emission times are observed for positive and negative pions due to similar values of R_{out} and different values of R_{side} for $\pi^+\pi^+$ and $\pi^-\pi^-$. The R_{out}, R_{side} and R_{long} increase from peripheral to central collisions reflecting the increase of the overlapping region of colliding nuclei.

The $R^2_{out-long}$ is found to be asymmetric with respect to the $y_{cm} - y_{pair} = 0$ and has negative and positive values in the negative and positive rapidities, respectively. Clear rapidity dependence of $R^2_{out-long}$ is observed due to asymmetry in longitudinal direction. Decreasing of R_{side} with pair rapidity, and $R^2_{out-long}$ having finite values and changing sign with respect to midrapidity hints to the boost-invariance breaking.

5. Conclusions

We performed the femtoscopic analysis of positively and negatively charged pion pairs produced in Au+Au collisions at $\sqrt{s_{NN}} = 3$ GeV. It was found that the correlation functions of positive and negative pions differ slightly at low pair transverse momentum, k_T, that may be due to the interaction with residual electric charge or different resonance decay contributions. The R_{out}, R_{side}, and R_{long} decrease with increasing transverse momentum of the pair due to transverse flow. We present the first measurement of femtoscopic parameter dependence on the pair rapidity, $y_{cm} - y_{pair}$, for 0–10 %, 10–30 %, 30–50 % central Au+Au collisions at $\sqrt{s_{NN}} = 3$ GeV.

The $R^2_{out-long}$ is negative for negative pair rapidities and positive for positive rapidities (crossing zero at midrapidity) due to the symmetry in the longitudinal direction. The decrease of R_{side} with increasing pair rapidity as well as the behavior of $R^2_{out-long}$ show a hint of boost-invariance breaking.

The R_{side} differs for positive and negative pion pairs, while the R_{out} values are similar, which may indicate a longer emission time for positive pions.

6. Patents

Author Contributions:

Funding: The work was funded in part by the Ministry of Science and Higher Education of the Russian Federation, Project "New Phenomena in Particle Physics and the Early Universe" FSWU-2023-0073, and by the MEPhI Program Priority 2030.

Institutional Review Board Statement:

Informed Consent Statement:

Data Availability Statement:

Acknowledgments: The work was partially performed using resources of the heterogeneous computing platform HybriLIT of JINR (LIT) (http://hlit.jinr.ru) and NRNU MEPhI high-performance computing center. Authors are grateful to Richard Lednický for fruitful discussions.

Conflicts of Interest:

References

1. I. Arsene et al. (BRAHMS Collaboration), Quark Gluon Plasma an Color Glass Condensate at RHIC? The perspective from the BRAHMS experiment. *Nucl. Phys. A* **2005**, *757*, 1.
2. K. Adcox et al. (PHENIX Collaboration), Formation of dense partonic matter in relativistic nucleus-nucleus collisions at RHIC: Experimental evaluation by the PHENIX collaboration. *Nucl. Phys. A* **2005**, *757*, 184.
3. B. B. Back et al. (PHOBOS Collaboration), The PHOBOS perspective on discoveries at RHIC. *Nucl. Phys. A* **2005**, *757*, 28.
4. J. Adams et al. (STAR Collaboration), Experimental and Theoretical Challenges in the Search for the Quark Gluon Plasma: The STAR Collaboration's Critical Assessment of the Evidence from RHIC Collisions. *Nucl. Phys. A* **2005**, *757*, 102.
5. J. Cleymans and K. Redlich, Chemical and thermal freeze-out parameters from 1A to 200A GeV. *Phys. Rev. C* **1999**, *60*, 054908.
6. F. Becattini, J. Manninen, and M. Gazdzicki, Energy and system size dependence of chemical freeze-out in relativistic nuclear collisions. *Phys. Rev. C* **2006**, *73*, 044905.
7. A. Andronic, P. Braun-Munzinger, and J. Stachel, Hadron production in central nucleus-nucleus collisions at chemical freeze-out. *Nucl. Phys. A* **2006**, *772*, 167.
8. K. Rajagopal and F. Wilczek, The Condensed Matter Physics of QCD. arXiv hep-ph/0011333 **2000**
9. E. Laermann and O. Philipsen, The Status of Lattice QCD at Finite Temperature. *Ann. Rev. Nucl. Part. Sci.* **2003**, *53*, 163.
10. M. Stephanov, QCD phase diagram: an overview. *PoS LAT2006* **2006**, *024*.
11. M. M. Aggarwal et al. (STAR collaboration), An Experimental Exploration of the QCD Phase Diagram: The Search for the Critical Point and the Onset of Deconfinement. *arXiv:1007.2613* **2010**.
12. K. Ackermann et al. (STAR Collaboration), STAR detector overview. *Nucl. Instrum. and Meth. A* **2003**, *499*, 624.
13. D. Boal, C. Gelbke, B. Jennings, Intensity interferometry in subatomic physics. *Rev. Mod. Phys.* **1990**, *62*, 553.
14. W. Bauer, C. Gelbke, S. Pratt, Hadronic interferometry in heavy ion collisions. *Annu. Rev. Nucl. Part. Sci.* **1992**, *42*, 77.
15. U. Heinz, B. Jacak, Two-Particle Correlations in Relativistic Heavy-Ion Collisions. *Annu. Rev. Nucl. Part. Sci.* **1999**, *49*, 529.
16. U. Wiedemann, U. Heinz, Particle Interferometry for Relativistic Heavy-Ion Collisions. *Phys. Rep.* **1999**, *319*, 145.
17. T. Csorgo, Particle Interferometry from 40 MeV to 40 TeV. *Heavy Ion Phys.* **2002**, *15*, 1.
18. G. Alexander, Bose-Einstein and Fermi-Dirac Interferometry in Particle Physics. *Rep. Prog. Phys.* **2003**, *66*, 481.
19. R. Hanbury-Brown, R. Twiss, A Test of a New Type of Stellar Interferometer on Sirius. *Nature* **1956**, *178*, 1046.
20. R. Hanbury-Brown, R. Twiss, A new type of interferometer for use in radio astronomy. *Philos. Mag.* **1954**, *45*, 663.
21. G. Goldhaber, S. Goldhaber, W. Lee, A. Pais, Influence of Bose-Einstein Statistics on the Antiproton-Proton Annihilation Process. *Phys. Rev.* **1960**, *120*, 300.
22. G. Kopylov, M. Podgoretsky, Correlations of identical particles emitted by highly excited nuclei. *Sov. J. Nucl. Phys.* **1972**, *15*, 219.
23. G. Kopylov, V. Lyuboshits, M. Podgoretsky, Correlations Between the Particles Which Have Small Relative Momenta. *JINR-P2-8069* **1974**.
24. G. Kopylov, M. Podgoretsky, Multiple production and interference of particles emitted by moving sources. *Sov. J. Nucl. Phys.* **1974**, *18*, 336.
25. G. Kopylov, Like particle correlations as a tool to study the multiple production mechanism. *Phys. Lett. B* **1974**, *50*, 472.
26. S. Koonin, Proton pictures of high-energy nuclear collisions. *Phys. Lett. B* **1977**, *70*, 43.
27. S.E. Koonin, Proton pictures of high-energy nuclear collisions. *Phys. Lett. B* **1977**, *70*, 43.
28. M. Gyulassy, S.K. Kauffmann and L.W. Wilson, Pion interferometry of nuclear collisions. I. Theory. *Phys. Rev. C* **1979**, *20*, 2267.
29. R. Lednicky and V. Lyuboshitz, Final state interaction effect on pairing correlations between particles with small relative momenta. *Sov. J. Nucl. Phys.* **1982**, *35*, 770.
30. D.H. Boal, C.-K. Gelbke, and B.K. Jennings, Intensity interferometry in subatomic physics. *Rev. Mod. Phys.* **1990**, *62*, 55.
31. M.G. Bowler, Coulomb corrections to Bose-Einstein corrections have greatly exaggerated. *Phys. Lett. B* **270**, *91*, 69.
32. Yu.M. Sinyukov, R. Lednicky, S.V. Akkelin, J. Pluta, B. Erazmus, Coulomb corrections for interferometry analysis of expanding hadron systems. *Phys. Lett. B* **1998**, *432*, 248.
33. L. Adamczyk *et al.*, Measurement of interaction between antiprotons. *Nature* **2016**, *527*, 345.
34. L. Fabbietti, V. Mantovani Sarti, and O. Vazquez Doce, Study of the Strong Interaction Among Hadrons with Correlations at the LHC. *Annu. Rev. Nucl. Part. Sci.* **2021**, *71*, 377.
35. R. Lednicky, V.L. Lyuboshitz, B. Erazmus, D. Nouais, How to measure which sort of particles was emitted earlier and which later. *Phys. Lett. B* **1996**, *373*, 30.

36. S. Voloshin, R. Lednicky, S. Panitkin, and N. Xu, Relative space-time asymmetries in pion and nucleon production in noncentral nucleus-nucleus collisions at high energies. *Phys. Rev. Lett.* **1997**, *79*, 4766.
37. D. Ardouin *et al.*, Unlike particle correlations and the strange quark matter distillation process. *Phys. Lett. B* **1999**, *446*, 191.
38. J. Bjorken, Highly relativistic nucleus-nucleus collisions: The central rapidity region. *Phys. Rev. D* **1983**, *27*, 140.
39. B. Back et. al. (PHOBOS Collaboration), The PHOBOS Perspective on Discoveries at RHIC. *Nucl. Phys. A* **2005**, *757*, 28.
40. S. Akkelin and Yu.M. Sinyukov, The HBT-interferometry of expanding sources. *Phys. Lett. B* **1995**, *356*, 525.
41. G. Bertsch, G. Brown, V. Koch and B. Li, Pion collectivity in relativistic heavy-ion collisions. *Nucl. Phys. A* **1988**, *490*, 3.
42. S. Pratt, Pion Interferometry for Exploding Sources. *Phys. Rev. Lett.* **1984**, *53*, 1219.
43. M. Bowler, Extended sources, final state interactions and Bose-Einstein correlations. *Z. Phys. C* **1988**, *39*, 81.
44. M. Bowler, Coulomb corrections to Bose-Einstein corrections have greatly exaggerated. *Phys. Lett. B* **1991**, *270*, 69.
45. Y. Sinyukov, R. Lednicky, S. Akkelin, J. Pluta, and B. Erazmus, Coulomb corrections for interferometry analysis of expanding hadron systems. *Phys. Lett. B* **1998**, *432*, 248.
46. R. Barlow, Systematic Errors: facts and fictions. *arXiv:hep-ex/0207026* **2002**.